Precision Medication 2 (2025) 100063

Contents lists available at ScienceDirect

Precision Medication

journal homepage: www.keaipublishing.com/en/journals/precision-medication/

Multi-omics mendelian randomization identifies ferroptosis-related genetic variants linked to NAFLD risk

Xiao Liu[a,b], Huadi Zhou[a,b], Chenhan Shou[a,b], Weifeng Wu[b], Yizhong Bao[c], Ying Yuan[d], Jianjun Zhang[b], Yue Zhang[b], Xiaohu Yang[b], Zhen Wang[e,*]

[a] The Fourth Clinical Medical School of Zhejiang Chinese Medical University,Hangzhou, China
[b] Zhejiang Hospital, Hangzhou, China
[c] Zhejiang Key Laboratory of Geriatrics and Geriatrics Institute of Zhejiang Province, Zhejiang Hospital, Hangzhou 310030, China
[d] Radiology Department of Beijing Friendship Hospital Affiliated to Capital Medical University, Beijing, China
[e] Hangzhou First People's Hospital, Hangzhou, China

ARTICLE INFO

Keywords:
Non-Alcoholic Fatty Liver Disease
Ferroptosis
Multi-Omics
Mendelian Randomization Analysis
Quantitative Trait Loci
DNA Methylation
Genome-Wide Association Study

ABSTRACT

Background: Ferroptosis, an iron-dependent cell death, contributes to non-alcoholic fatty liver disease (NAFLD), but causal genes remain unclear. This study identifies ferroptosis-related genes driving NAFLD to fill this gap.
Methods: Summary data-based Mendelian Randomization (SMR) analyzed 564 ferroptosis-related genes for causal links to NAFLD by integrating mQTL/eQTL/pQTL data with GWAS, validated in FinnGen and the GWAS Catalog. To further substantiate our findings, expression of lead candidate genes was validated in independent human liver tissue datasets from the Gene Expression Omnibus (GEO). HepG2 cells were used to assess candidate gene expression, oxidative stress, and ferroptosis under free fatty acids (FFA) treatment. We evaluated cell viability, lipid ROS levels, gene expression, protein levels, and oxidative stress markers.
Results: SMR analysis revealed an association between *SLC2A6* methylation/expression and NAFLD risk. Hypermethylation at cg02257517 was associated with increased NAFLD risk (OR = 1.032, 95 % CI = 1.013–1.051), while higher *SLC2A6* expression correlated with lower risk (OR = 0.919, 95 % CI = 0.87–0.97). Multi-omics analysis confirmed an inverse relationship between *SLC2A6* expression and cg02257517 methylation (OR = 0.741, 95 % CI = 0.66–0.832), suggesting hypermethylation downregulates *SLC2A6*, increasing NAFLD susceptibility. Those results were further validated in HepG2 cells, where the candidate gene demonstrated a protective role against FFA-induced oxidative stress and ferroptosis. Overexpression of the gene significantly mitigated these pathological effects, supporting its potential as a therapeutic target.
Conclusion: Multi-omics Mendelian randomization identified SLC2A6 hypermethylation as a causal NAFLD risk factor by suppressing its expression. Functional validation in disease-relevant models revealed SLC2A6-mediated protection against oxidative stress and ferroptosis, highlighting its potential as a therapeutic target for NAFLD through epigenetic or gene-based interventions.

Introduction

Non-alcoholic fatty liver disease (NAFLD) is a common liver disorder characterized by excessive fat accumulation in the liver without alcohol involvement.[1] It spans a spectrum from simple steatosis to non-alcoholic steatohepatitis (NASH),[2] which can progress to liver fibrosis, cirrhosis, and hepatocellular carcinoma.[3] Although ferroptosis has been implicated in the pathogenesis of NAFLD, the specific ferroptosis-related genes that are causally linked to NAFLD remain poorly understood. Current studies have primarily focused on observational associations, lacking definitive evidence of causal relationships. Therefore, the primary goal of this study is not to exhaustively map the downstream metabolic pathways, but to leverage a genetic-based approach to identify high-confidence causal gene candidates that link ferroptosis to NAFLD risk. This study aims to address this gap by using summary data-based Mendelian randomization (SMR) analysis combined with multi-omics data to systematically explore the potential causal links between ferroptosis-related genes and NAFLD. Hepatic iron

* Corresponding author.
E-mail address: wangzhen@hospital.westlake.edu.cn (Z. Wang).

https://doi.org/10.1016/j.prmedi.2025.100063
Received 4 June 2025; Received in revised form 5 August 2025; Accepted 20 August 2025
Available online 12 December 2025

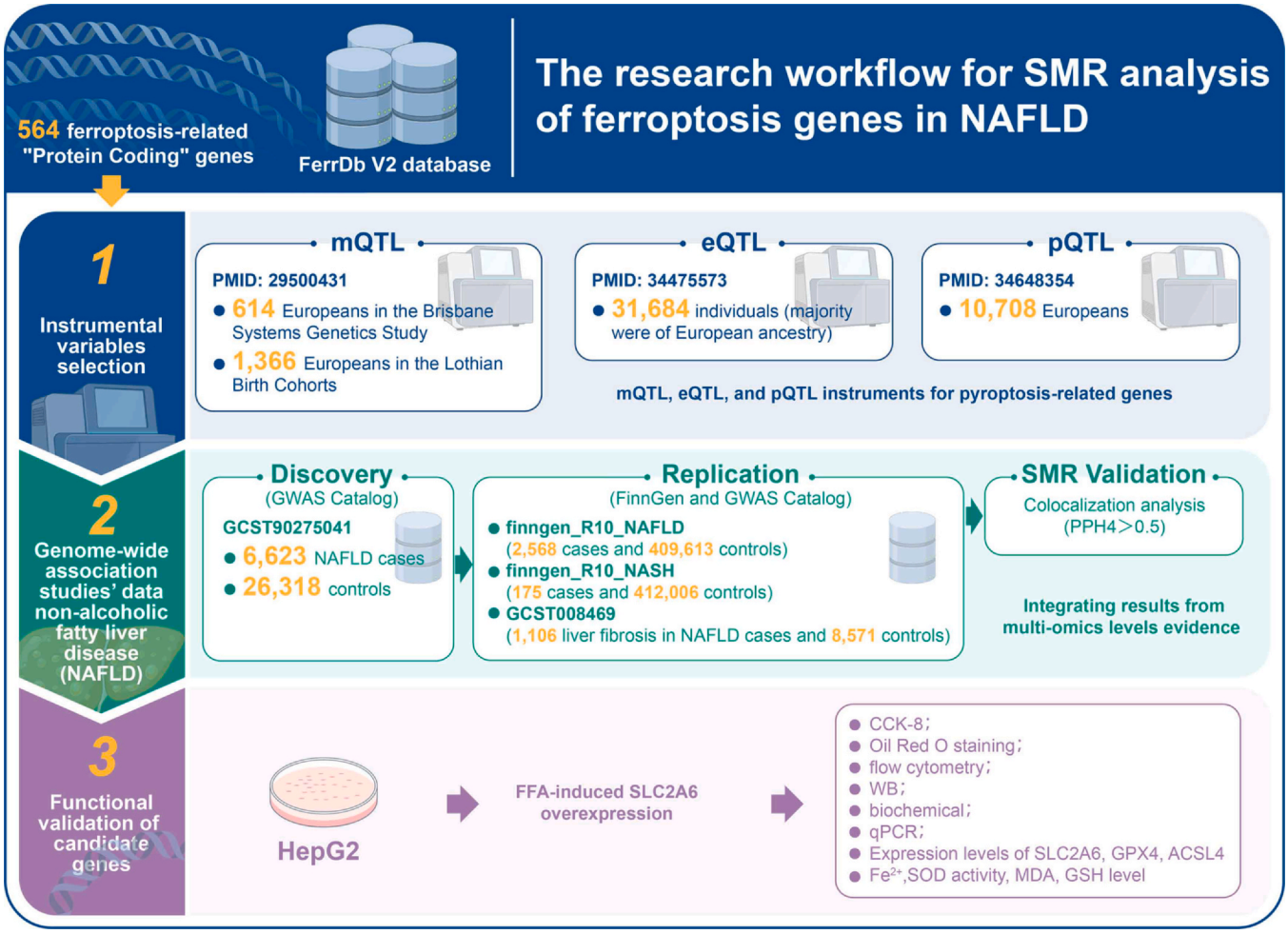

Fig. 1. Study workflow for identifying ferroptosis-related genes associated with NAFLD.

deposition plays a key role in NAFLD progression, as excess iron promotes oxidative stress, lipid peroxidation, and inflammation, accelerating the transition to NASH, fibrosis, and more severe outcomes.[4] NAFLD affects around 25 % of the global population,[5] with risk factors including obesity, type 2 diabetes, and metabolic syndrome.[6] Symptoms such as fatigue, abdominal discomfort, and liver-related complications can severely impact patients' quality of life.[7] Current treatments, such as lifestyle changes and pharmacological agents, provide limited benefits due to the absence of FDA-approved therapies and inconsistent efficacy, with no drugs effectively targeting all aspects of disease progression.[8] Given these limitations, genetic and epigenetic insights indicate the potential for individualized therapies that more precisely target the underlying mechanisms of NAFLD progression.[9] Identifying causal genetic factors, particularly those related to iron metabolism, is crucial for developing treatments that address the underlying mechanisms of NAFLD, particularly its progression to NASH and fibrosis.

NAFLD progression involves iron-induced oxidative stress and lipid peroxidation. Excessive iron accumulation in the liver promotes reactive oxygen species (ROS) formation via the Fenton reaction, leading to lipid peroxidation, hepatocyte damage, inflammation, and fibrosis, which accelerate the progression to NASH.[10] Iron overload also contributes to obesity and insulin resistance,[11] both of which are major risk factors for NAFLD. Ferroptosis, an iron-dependent cell death driven by lipid peroxidation, plays a significant role in the pathogenesis of NAFLD and its progression to NASH and liver fibrosis.[12] This process results from impaired antioxidant defenses, such as the inhibition of *glutathione peroxidase 4* (*GPX4*), and elevated iron levels, leading to oxidative stress.[13] Ferroptosis-related genes involved in lipid metabolism, iron homeostasis, and oxidative stress response have been identified as contributors to NAFLD, suggesting that dysregulation in these pathways may link ferroptosis to the onset and progression of NAFLD. However, the precise genetic and epigenetic mechanisms underlying these associations remain unclear.

Summary-data-based Mendelian Randomization (SMR) is an analytical method that combines genome-wide association studies (GWAS) data with molecular quantitative trait loci (QTL) data, such as methylation QTLs (mQTLs), expression QTLs (eQTLs), and protein QTLs (pQTLs), to identify causal genes and their regulatory mechanisms. This method uses genetic variants as instrumental variables to help clarify causal relationships and avoid confounding factors, providing insights into the genetic and epigenetic factors that contribute to complex diseases like NAFLD. SMR is particularly valuable for identifying genes whose changes in expression or regulation may directly influence disease risk and progression, offering potential therapeutic targets.[14] However, a significant challenge in such analyses is tissue specificity. Many large-scale QTL datasets are derived from accessible tissues like blood, and the genetic regulatory effects observed may not always reflect the specific biological context of the target organ, such as the liver in NAFLD. Therefore, validating findings in disease-relevant tissues is a critical step to confirm their biological plausibility.

This study aimed to identify ferroptosis-related causal genes for NAFLD and its progression using SMR analysis. We integrated methylation, expression, and protein data with GWAS to uncover molecular mechanisms linking genetic variation to NAFLD development. Validation was conducted using independent NAFLD, NASH, and liver fibrosis datasets, and integrative multi-omics analyses were performed

to further elucidate these mechanisms. To confirm the clinical relevance of our top candidates, we further validated their expression in liver tissue from independent patient cohorts. Our results may reveal critical ferroptosis-related genes that contribute to the development and progression of NAFLD, potentially offering new insights into the underlying molecular mechanisms and identifying novel therapeutic targets for intervention.

Methods

Study design

This study utilized a structured, multi-step workflow. Initially, SMR analysis was performed using data from the GWAS Catalog to identify potential ferroptosis-related genes associated with NAFLD by integrating mQTL, eQTL, and pQTL data with GWAS results. Colocalization analyses were conducted to determine whether the same genetic variants influenced both the QTLs and NAFLD risk. Next, SMR findings were validated using NAFLD and NASH datasets from the FinnGen project, as well as a liver-fibrosis-in-NAFLD dataset from the GWAS Catalog. Following this, integrative analyses across multiple omics layers were performed to uncover the molecular mechanisms linking genetic variation to NAFLD development. Finally, the association between ferroptosis-related gene expression and NAFLD risk was further evaluated using liver-specific eQTL data. The flowchart of the study is presented in Fig. 1.

Data sources of mQTLs, eQTLs, and pQTLs

A total of 564 ferroptosis-related genes were downloaded from the FerrDb V2 database.[15] Summary data for blood mQTL were derived from a meta-analysis of two European cohorts:[16] the Brisbane Systems Genetics Study (n = 614) and the Lothian Birth Cohorts (n = 1366). Blood eQTL data were obtained from the eQTLGen consortium,[17] comprising genetic data on blood gene expression from 31,684 European individuals. Blood pQTL data were sourced from a previous study,[18] including 10,708 European individuals. The association between ferroptosis-related gene expression and NAFLD risk was evaluated using liver-specific eQTL data from The Genotype-Tissue Expression (GTEx) V8 database, which consists of data from 838 donors and includes 17,382 samples from 52 tissues and two cell lines.[19]

NAFLD outcome datasets

The NAFLD discovery dataset GCST90275041 was obtained from the GWAS Catalog, including 6623 European ancestry cases and 26,318 European ancestry controls.[20] For validation, NAFLD (2568 cases, and 409,613 controls) and NASH datasets (175 cases and 412,006 controls) were sourced from the FinnGen project (R10 release), primarily consisting of individuals of Finnish ancestry. Additionally, a liver-fibrosis-in-NAFLD dataset (GCST008469) of European ancestry (1106 cases and 8571 controls) was sourced from the GWAS Catalog.[21] The dataset details are summarized in Table S1.

SMR analysis

To identify ferroptosis-related genes associated with NAFLD, SMR analyses and heterogeneity in dependent instruments (HEIDI) tests were conducted using the SMR software tool (SMR v1.3.1) as previously described.[22,23] The primary aim was to investigate the relationships between ferroptosis-related gene methylation, expression, and protein abundance with NAFLD. The SMR approach combined summary-level GWAS with mQTL, eQTL, and pQTL data to identify pleiotropic associations suggestive of causal relationships, while the HEIDI test identified whether shared genetic variation influences both exposure and outcome by analyzing associations across multiple SNPs within a region. We focused on top associated cis-QTLs within a ± 1000 kb window around the gene to identify relevant genetic variants, applying a P-value threshold of 5.0×10^{-8} to ensure robust associations. SNPs with allele frequency differences greater than 0.2 between datasets, including LD reference samples, QTL summary data, and outcome summary data, were excluded, maintaining a maximum allowable proportion of 0.05. To enhance the robustness of our findings, SMR_multi was employed to incorporate multiple genetic variants simultaneously, with significance thresholds at $p < 0.05$ for both SMR and SMR_multi analyses. The HEIDI test threshold was set at $p\_HEIDI > 0.01$ to exclude associations due to linkage disequilibrium.

Integration of multi-omics evidence

To identify the key ferroptosis gene in NAFLD, we conducted an integrative analysis across mQTL, eQTL, and pQTL data. To test pleiotropic associations, we used mQTL and eQTL summary data in BESD format, focusing on cis-regions within a ± 1000 kb distance between genes and DNA methylation sites. Specifically, we examined the causal relationships between gene methylation and expression, gene expression, and protein levels, and linked these to NAFLD risk by integrating with GWAS data. $p\_SMR < 0.05$, $p\_SMR\_multi < 0.05$, and $p\_HEIDI > 0.01$ were applied to determine significant associations.

Colocalization analysis

To determine whether the observed associations in both traits are driven by the same genetic variants, we employed Bayesian colocalization analysis. This approach is favored for its ability to account for various sources of variation, providing a more reliable framework compared to other methods.[24] By evaluating the probability that a single genetic variant affects both QTL and GWAS traits, this method offers evidence of a shared genetic basis. Significant associations ($p\_SMR\_multi < 0.05$, $p\_SMR < 0.05$, and $p\_HEIDI > 0.01$) were further examined using the R package 'coloc' to identify shared genetic variants between cis-QTLs and NAFLD.[25] Additionally, SNPs within ± 1000 kb of the top cis-QTLs colocalization region windows were analyzed. Five distinct hypotheses (H0–H4) were tested: no association with either trait (H0), association with only the first trait (H1), association with only the second trait (H2), association with both traits but with different causal variants (H3), and association with both traits sharing the same causal variant (H4). A posterior probability (PPH4) greater than 0.5 was considered a significant colocalization.[26]

Validation of gene expression in an independent liver tissue cohort

To validate the expression of our key candidate genes in a clinically relevant tissue, we analyzed the publicly available RNA-sequencing dataset GSE126848 from the Gene Expression Omnibus (GEO) database. This dataset contains expression profiles from human liver biopsies. Based on the study's design, we specifically selected samples from 15 non-alcoholic fatty liver (NAFL) patients and 14 healthy normal-weight individuals for our validation analysis. The expression data, formatted as Transcripts Per Million (TPM), were utilized to assess the differential expression of *SLC2A6* and *MAPKAP1* between the NAFL and healthy control groups using a Wilcoxon test. The results were subsequently visualized as a boxplot.

Cell culture and transfection

HepG2 cells were cultured in DMEM (Gibco, Thermo Fisher Scientific, Waltham, MA, USA) supplemented with 10 % fetal bovine serum (FBS; Gibco) and 1 % penicillin-streptomycin solution (Solarbio, Beijing, China) at 37°C in a humidified atmosphere containing 5 % CO_2. Cells in the logarithmic growth phase were trypsinized and seeded at a density of 2×10^6 cells per well in a 6-well plate. For *SLC2A6*

overexpression, cells were transfected with oe-SLC2A6 plasmids using Lipofectamine 2000 (Thermo Fisher Scientific) following the manufacturer's instructions. Cells were harvested 48 h post-transfection for further analyses.

Plasmid construction

The SLC2A6 coding sequence (CDS, NM_017585.4) was synthesized and cloned into the pcDNA3.1(+) vector (Addgene) using Hind III and EcoR I restriction sites (Thermo Fisher Scientific). The recombinant plasmid (pcDNA3.1-SLC2A6) was verified by bidirectional Sanger sequencing (General Biosystems, Anhui, China). The full plasmid sequence, including CMV promoter, SLC2A6 CDS, and BGH polyadenylation signal, is provided in Table S2.

Cell counting kit-8 (CCK-8) assay

Cell viability was assessed using the CCK-8 assay (Beyotime, Shanghai, China) following the manufacturer's protocol. HepG2 cells were seeded into 96-well plates at a density of 8×10^3 cells per well and incubated overnight. The next day, cells were treated with free fatty acids (FFA) (Xi'an Kunchuang Technology, Xi'an, China) or left untreated as a control. After 24 h, CCK-8 reagent was added to each well at a 1:10 dilution in serum-free medium, followed by incubation at 37°C for 1 h. Absorbance was measured at 450 nm using a microplate reader (Beijing Pulang New Technology Co., Ltd., Beijing, China). Each condition was tested in triplicate.

qRT-PCR

HepG2 cells were treated as above mentioned. qRT-PCR was performed using the SLAN-965 real-time PCR system (Shanghai Hongshi Medical Technology Co., Ltd., Shanghai, China). Total RNA was extracted using the total RNA extraction reagent (Solarbio) and reverse transcribed into cDNA with the all-in-one first-strand cDNA synthesis kit (TransGen Biotech, Beijing, China). qRT-PCR was conducted using the 2 ×Q3 SYBR qPCR master mix (universal) (TransGen Biotech) according to the manufacturer's protocol. The following primers were used: *SLC2A6* (Forward: CCCTGCAGAACAAAAGGGTG, Reverse: CAG GATGCCTGGGATTTGGT, product size: 154 bp) and *GAPDH* (Forward: GAAGGTCGGAGTCAACGGAT, Reverse: CTTCCCGTTCTCAGCCATGT, product size: 133 bp). GAPDH was used as an internal control, and gene expression was quantified using the ΔΔCT method. Each reaction was performed in triplicate.

Western blot analysis

Western blotting was performed to analyze protein expression using the mini-PROTEAN 3 cell system (Bio-Rad, Hercules, CA, USA). Protein concentration was determined using the BCA protein assay kit (Thermo Fisher Scientific). Equal amounts of protein were separated by SDS-PAGE on 10 % or 12 % polyacrylamide gels, depending on the target protein size, and transferred onto nitrocellulose membranes (Millipore, Burlington, MA, USA) using a semi-dry transfer system (PS-9; Dalian Jingmai Technology Co., Ltd., Dalian, China). Membranes were blocked with 5 % non-fat milk in TBST and incubated overnight at 4°C with primary antibodies: SLC2A6 (1:1000, Abcam, Cambridge, UK; ab135924), GPX4 (1:1000, Abcam; ab125066), ACSL4 (1:1000, Abcam; ab155282), and GAPDH (1:8000, Proteintech, Wuhan, China; 60004–1-AP). After washing, membranes were incubated with HRP-conjugated secondary antibodies (1:10,000, Zhongshan Golden Bridge, Beijing, China) at 37°C for 1 h. Protein bands were detected using ECL reagent (Millipore) and visualized using the Tanon-5200 imaging system (Tanon, Shanghai, China). Densitometric analysis was performed using ImageJ software.

Oil Red O staining

Oil Red O staining was performed to visualize intracellular lipid accumulation. HepG2 cells were seeded onto glass coverslips in 12-well plates and allowed to adhere overnight. After treatment with FFA for 24 h, cells were fixed in 10 % formalin (Solarbio) for 10 min at room temperature and washed with distilled water. Cells were then incubated in 60 % isopropanol (Sinopharm, Shanghai, China) for 30 s, followed by staining with freshly prepared Oil Red O working solution (Solarbio) for 10–15 min at room temperature. Excess stain was removed by rinsing with 60 % isopropanol, and cells were counterstained with Mayer's hematoxylin (Beijing Leigen, Beijing, China) for 1–2 min to visualize nuclei. After thorough washing in running water (10 min), coverslips were mounted with glycerol gelatin (Solarbio) and observed under a light microscope (Nikon ECLIPSE Ni, Tokyo, Japan). Representative images were captured using a DS-Ri2 imaging system (Nikon).

Flow cytometry

Flow cytometry was used to detect lipid reactive oxygen species (ROS) levels in HepG2 cells. After treatment, cells were washed twice with PBS, trypsinized, and centrifuged at 1000 rpm for 5 min to collect the cell pellet. The cells were then incubated with 10 μM BODIPY 581/591 C11 probe (MCE, USA; HY-D1301) in the dark at 37°C for 30 min. After incubation, cells were washed three times with PBS and analyzed using the CytoFLEX flow cytometer (Beckman Coulter, USA). Mean fluorescence intensity (MFI) was used to quantify lipid ROS levels.

Biochemical assays for oxidative stress and ferroptosis markers

Lipid peroxidation, antioxidant activity, and ferroptosis markers were assessed in cell lysates using commercial assay kits. Malondialdehyde (MDA) levels were measured using a TBA assay kit (Nanjing Jiancheng Bioengineering Institute, Nanjing, China; A003–1) at 532 nm. Superoxide dismutase (SOD) activity was determined with a xanthine oxidase-based assay kit (Nanjing Jiancheng; A001) at 550 nm. Glutathione (GSH) levels were quantified using a DTNB assay kit (Solarbio; BC1175) at 412 nm. Fe^{2+} content was measured using a ferrous ion detection kit (Solarbio; BC5415) at 593 nm. Cells were lysed, and supernatants were collected by centrifugation at 10,000–12,000 g for 10 min at 4°C. Absorbance was recorded using a microplate reader (Beijing Pulang New Technology Co., Ltd.), and results were normalized to protein content.

Statistical analysis

All statistical analyses were performed using R (v4.3.0). Manhattan plots and forest plots were generated using the "ggplot2" and "forestplot" packages, respectively. The SMRLocusPlot and SMREffectPlot functions were adapted from a previous study.[27]

Results

Ferroptosis-related gene methylation and NAFLD

SMR analysis of mQTLs (Table S3) identified 85 methylation sites associated with NAFLD across 43 ferroptosis-related genes in the GCST90275041 cohort. A total of 30 loci corresponding to 21 genes exhibited significant colocalization evidence (PPH4 > 0.5) (Fig. 2). For example, *SLC2A6* (cg02257517) displayed a significant positive association with NAFLD risk (OR = 1.032, 95 % CI = 1.013–1.051, *p*_SMR = 0.00106, *p*_SMR_multi = 0.00513, PPH4 = 0.919), suggesting that methylation at this locus in *SLC2A6* may contribute to an increased risk of NAFLD. The SMR analysis in the FinnGen NAFLD cohort validated 6 methylation loci: *PANX1* (cg01091143), *PANX1* (cg02814482), *PPARG* (cg04632671), *PRKCA* (cg15519474), *SLC39A14*

probeID	Gene	OR (95%CI)	p_SMR	p_SMR_multi	PPH4
cg15799267	ALOX15B	0.96(0.932 - 0.99)	0.00818	0.008183	0.838 *
cg21071793	ATG7	1.025(1.007 - 1.043)	0.00578	0.024472	0.538 *
cg07954885	BRD2	1.034(1.01 - 1.058)	0.00569	0.005693	0.838 *
cg26246658	BRD2	1.038(1.011 - 1.066)	0.00643	0.00643	0.835 *
cg01962969	CBR1	0.993(0.987 - 0.999)	0.0135	0.013496	0.676 *
cg03841977	CBR1	0.992(0.986 - 0.998)	0.01357	0.034284	0.676 *
cg05297739	CBR1	1.02(1.004 - 1.037)	0.01573	0.015734	0.675 *
cg16662267	CBR1	0.993(0.987 - 0.999)	0.0135	0.0008665	0.676 *
cg16719517	CBR1	0.993(0.988 - 0.999)	0.01346	0.048201	0.676 *
cg06047934	CHMP1A	1.032(1.012 - 1.052)	0.00171	0.0005074	0.587 *
cg22314562	CHMP1A	1.041(1.008 - 1.076)	0.0154	0.015403	0.848 *
cg16915659	CISD1	1.027(1.006 - 1.048)	0.01015	0.010147	0.615 *
cg07593977	CTSB	1.046(1.01 - 1.084)	0.01227	0.012266	0.648 *
cg01079242	DPEP1	0.967(0.943 - 0.992)	0.0111	0.011103	0.522 *
cg08939942	FZD7	1.04(1.011 - 1.07)	0.00714	0.007141	0.714 *
cg23841344	HSD17B11	0.984(0.974 - 0.995)	0.00439	0.034133	0.778 *
cg03741506	OTUB1	1.027(1.003 - 1.051)	0.02701	0.017479	0.552 *
cg01091143	PANX1	0.975(0.956 - 0.994)	0.01137	0.009434	0.532 *
cg08246316	PHKG2	0.973(0.955 - 0.992)	0.00446	0.004458	0.699 *
cg04632671	PPARG	1.041(1.014 - 1.07)	0.00327	0.003272	0.746 *
cg15519474	PRKCA	0.971(0.949 - 0.994)	0.01375	0.013747	0.623 *
cg25909396	PRKCA	0.963(0.934 - 0.993)	0.01736	0.017362	0.703 *
cg20500836	RPTOR	1.013(1.002 - 1.024)	0.02029	0.021055	0.576 *
cg02257517	SLC2A6	1.032(1.013 - 1.051)	0.00106	0.00513	0.919 *
cg05254747	SLC39A14	1.057(1.02 - 1.096)	0.0026	0.0026	0.939 *
cg05536998	SMAD7	0.974(0.956 - 0.992)	0.0045	0.004503	0.56 *
cg15347961	SNX5	1.048(1.013 - 1.083)	0.00605	0.006052	0.808 *
cg06400745	TRIM26	1.03(1.006 - 1.055)	0.01374	0.013744	0.598 *
cg15018282	TRIM26	1.045(1.007 - 1.083)	0.01853	0.018528	0.588 *
cg21666768	TRIM26	1.028(1.004 - 1.053)	0.02111	0.021108	0.589 *

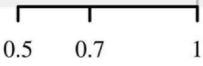

Fig. 2. SMR analysis of ferroptosis-related gene methylation associated with NAFLD risk in the GCST90275041 cohort. The forest plot shows 30 methylation loci across 21 ferroptosis-related genes associated with NAFLD, with colocalization evidence (PPH4 > 0.5). The horizontal lines represent the 95 % confidence intervals (CI) for the odds ratios (OR). OR: odds ratio; 95 % CI: 95 % confidence intervals; PPH4: posterior probability of colocalization. *Significant colocalization (PPH4 > 0.5).

(cg02479022), and *SMAD7* (cg05536998). In the FinnGen NASH cohort, 4 methylation loci were validated, including *PEX10* (cg12715395), *PEX10* (cg02610723), *PEX10* (cg06007201), and *PIEZO1* (cg27004870). Additionally, *CREB5* (cg10421188) was validated in the liver fibrosis cohort (Table S4). All external validation results are summarized in Tables S5, S6,and S7.

Ferroptosis-related gene expression and NAFLD

SMR analysis of eQTLs (Table S3) identified 10 ferroptosis-related genes significantly associated with NAFLD risk in the GCST90275041 cohort (Fig. S1), including *ALOX12, ATG13, ATG7, CDKN2A, GCH1, GLS2, MAPKAP1, PARP8, PRKCA,* and *SLC2A6*. Among these, five genes (*ATG7, CDKN2A, GCH1, PRKCA,* and *SLC2A6*) showed significant colocalization evidence (PPH4 > 0.5). Specifically, *ATG7* (OR = 1.043, 95 % CI = 1.016–1.071, *p*_SMR = 0.018, *p*_SMR_multi = 0.010252, PPH4 = 0.7171) and *PRKCA* (OR = 1.049, 95 % CI = 1.018–1.081, *p*_SMR = 0.00177, *p*_SMR_multi = 0.001492, PPH4 = 0.7443) were positively correlated with NAFLD risk, while *CDKN2A* (OR = 0.92, 95 % CI = 0.86–0.984, *p*_SMR = 0.01536, *p*_SMR_multi = 0.029425, PPH4 = 0.5381), *GCH1* (OR = 0.973, 95 % CI = 0.955–0.991, *p*_SMR = 0.00322, *p*_SMR_multi = 0.018389, PPH4 = 0.8996), and *SLC2A6* (OR = 0.919, 95 % CI = 0.87–0.97, *p*_SMR = 0.00234, *p*_SMR_multi = 0.0001745, PPH4 = 0.9295) were negatively correlated.

Table 1
Integration of mQTL and eQTL SMR analyses revealed potential associations between the methylation of *ALOX12, MAPKAP1,* and *SLC2A6* and their expression.

Expo_ID	Outco_Gene	SYMBOL	*p*_SMR	*p*_SMR_multi	OR_SMR	95 % CI_SMR
cg20216752	ENSG00000108839	ALOX12	9.05E-14	9.05E-14	1.493	1.343–1.658
cg27410136	ENSG00000108839	ALOX12	2.38E-09	2.38E-09	1.708	1.433–2.036
cg11299964	ENSG00000119487	MAPKAP1	8.14E-10	8.14E-10	0.655	0.572–0.75
cg02257517	ENSG00000160326	SLC2A6	4.14E-07	3.32E-06	0.741	0.66–0.832

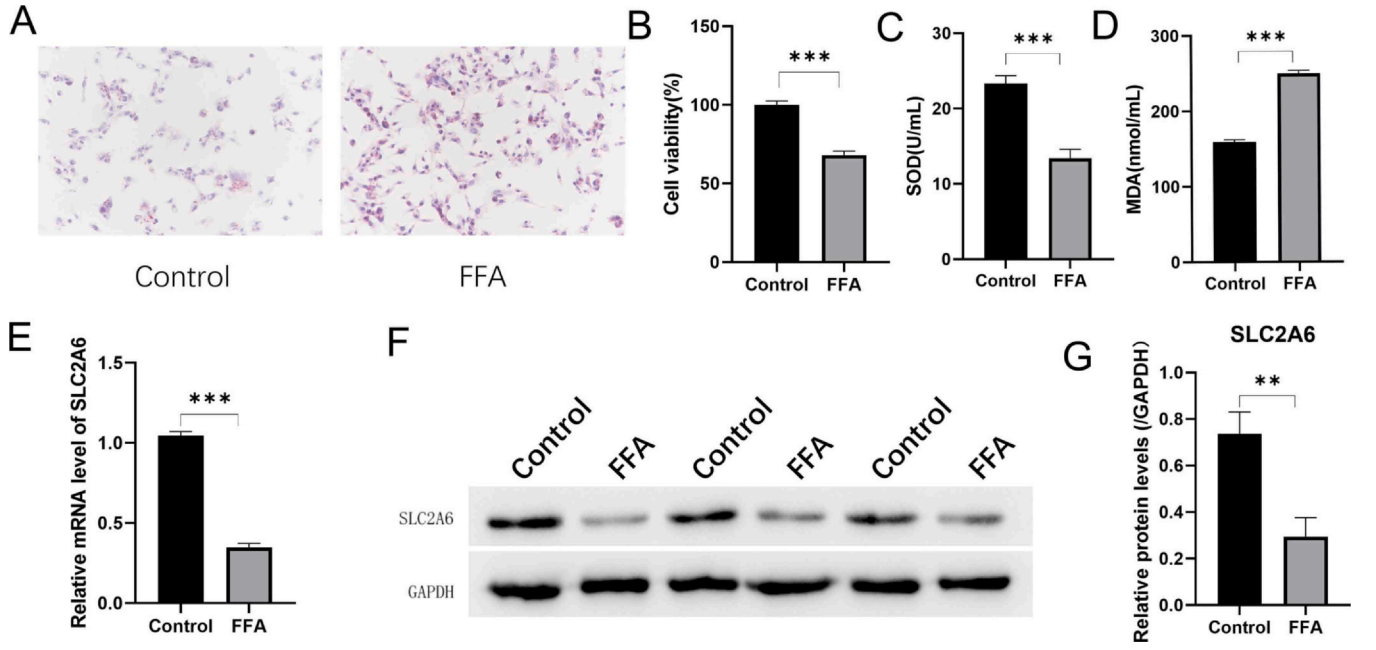

Fig. 3. *SLC2A6* expression and lipid accumulation in free fatty acids (FFA)-treated HepG2 cells. (A) Representative images of Oil Red O staining in control and FFA-treated HepG2 cells. (B) CCK-8 assay for cell viability in control and FFA-treated cells. (C, D) Superoxide dismutase (SOD) activity and malondialdehyde (MDA) levels in control and FFA-treated cells. (E) qRT-PCR analysis of *SLC2A6* mRNA expression in control and FFA-treated HepG2 cells. (F, G) Western blot analysis of SLC2A6 protein expression in FFA-treated cells compared to controls, with GAPDH as a loading control. Data are expressed as mean ± standard deviation. **p < 0.01, ***p < 0.001, n = 3.

However, these results were not validated in the external cohorts (Tables S5-7).

Ferroptosis-related protein abundance and NAFLD

SMR analysis of pQTLs (Table S3) identified two ferroptosis-related proteins significantly associated with NAFLD risk in the GCST90275041 cohort (Fig. S2). PRKCA (OR = 1.074, 95 % CI = 1.012–1.14, *p*_SMR = 0.0182, *p*_SMR_multi = 0.02441, PPH4 = 0.502) showed a positive correlation with NAFLD risk with significant colocalization evidence, and STAT3 (OR = 0.974, 95 % CI = 0.952–0.995, *p*_SMR = 0.018, *p*_SMR_multi = 0.00876, PPH4 = 0.334) showed a negative correlation with NAFLD risk without significant colocalization evidence. However, validation attempts in the external cohorts did not replicate these results (Tables S5-7).

Integration of multi-omics analyses

To test pleiotropic associations between molecular traits, we performed an integrative analysis. Integration of mQTL and eQTL summary data (Table S8) revealed significant associations between methylation and gene expression (Table 1). Manhattan plots highlighted these associations, showing significant peaks for *ALOX12, MAPKAP1,* and *SLC2A6* (Fig. S3A-C). Specifically, *ALOX12* showed positive associations at cg20216752 (OR = 1.493, 95 % CI = 1.343–1.658, *p*_SMR = 9.05E-14, *p*_SMR_multi = 9.05E-14) and cg27410136 (OR = 1.708, 95 % CI = 1.433–2.036, *p*_SMR = 2.38E-09, *p*_SMR_multi = 2.38E-09). Conversely, *MAPKAP1* exhibited a significant negative association at cg11299964 (OR = 0.655, 95 % CI = 0.572–0.75, *p*_SMR = 8.14E-10, *p*_SMR_multi = 8.14E-10), and *SLC2A6* showed a significant negative association at cg02257517 (OR = 0.741, 95 % CI = 0.66–0.832, *p*_SMR = 4.14E-07, *p*_SMR_multi = 3.32E-06). Importantly, *SLC2A6* was the only gene among the three that demonstrated colocalization support in both mQTL and eQTL analyses. The locus plots illustrated significant associations of genetic variants with *SLC2A6* methylation and expression levels (Fig. S4A and S4B). The effect size plots demonstrated a significant positive correlation between the GWAS and mQTL effect sizes at cg02257517 (Fig. S4C) and a significant negative correlation between the GWAS and eQTL effect sizes for *SLC2A6* expression (Fig. S4D). These data suggest that genetic variants associated with higher methylation at cg02257517 lead to decreased *SLC2A6* expression, which is associated with a higher risk of NAFLD. To directly address the issue of tissue specificity, we performed a validation analysis using the independent human liver tissue dataset GSE126848. This analysis confirmed the dysregulation of our key candidate genes in the context of NAFLD. Consistent with the protective role suggested by our SMR analysis, *SLC2A6* mRNA expression was found to be significantly downregulated in liver biopsies from patients with NAFL compared to healthy controls. Conversely, the expression of *MAPKAP1* was significantly upregulated in the same comparison (Figure S5). These findings from a clinical liver cohort provide strong, direct support for our primary results.

SLC2A6 overexpression reduces FFA-induced oxidative stress and ferroptosis in HepG2 cells

Given that *SLC2A6* methylation and expression were significantly associated with NAFLD risk, we investigated its function in hepatic lipid metabolism. HepG2 cells were treated with FFA to induce lipid accumulation, mimicking hepatic steatosis, and subsequently stained with Oil Red O to assess intracellular lipid deposition. Compared to the control group, FFA-treated cells exhibited a marked increase in lipid accumulation, confirming the successful establishment of a steatosis model (Fig. 3A). FFA treatment significantly reduced cell viability (Fig. 3B), decreased SOD activity (Fig. 3C), and increased MDA levels (Fig. 3D), indicating oxidative stress. qRT-PCR analysis revealed downregulated *SLC2A6* mRNA expression in FFA-treated cells (Fig. 3E), which was further confirmed at the protein level by Western blot (Fig. 3F, 3G). These results suggest that FFA exposure induces oxidative stress and downregulates *SLC2A6* expression, implicating its potential role in NAFLD pathogenesis.

To determine whether *SLC2A6* overexpression reverses FFA-induced oxidative stress and ferroptosis, we examined its impact on gene expression, cell viability, and oxidative stress markers. qRT-PCR and Western blot confirmed successful transfection, showing a significant increase in *SLC2A6* mRNA and protein levels (Fig. 4A). qRT-PCR revealed that FFA treatment downregulated SLC2A6 mRNA expression, while *SLC2A6* overexpression restored its expression despite FFA exposure (Fig. 4B). Cell viability assays indicated that FFA reduced viability, whereas *SLC2A6* overexpression rescued cell viability, suggesting a protective role against FFA-induced cytotoxicity (Fig. 4C). Flow cytometry analysis demonstrated increased lipid ROS levels in FFA-treated cells, which were significantly reduced by *SLC2A6* overexpression (Fig. 4D). MFI quantification confirmed this reduction (Fig. 4E). Western blot analysis showed that FFA treatment decreased GPX4 expression, which is involved in antioxidant defense, while increasing Acyl-CoA Synthetase Long Chain Family Member 4 (ACSL4), a ferroptosis maker. *SLC2A6* overexpression partially reversed these effects, suggesting a regulatory role in oxidative stress and ferroptosis (Fig. 4F). Furthermore, biochemical assays revealed that *SLC2A6* overexpression restored SOD and GSH levels while reducing MDA and Fe^{2+} accumulation (Fig. 4H). These findings suggest that *SLC2A6* regulates oxidative stress and ferroptosis in NAFLD, serving as a potential therapeutic target for alleviating FFA-induced hepatic injury.

Discussion

SMR analysis identified *SLC2A6* methylation and expression as significantly associated with NAFLD risk, with hypermethylation at

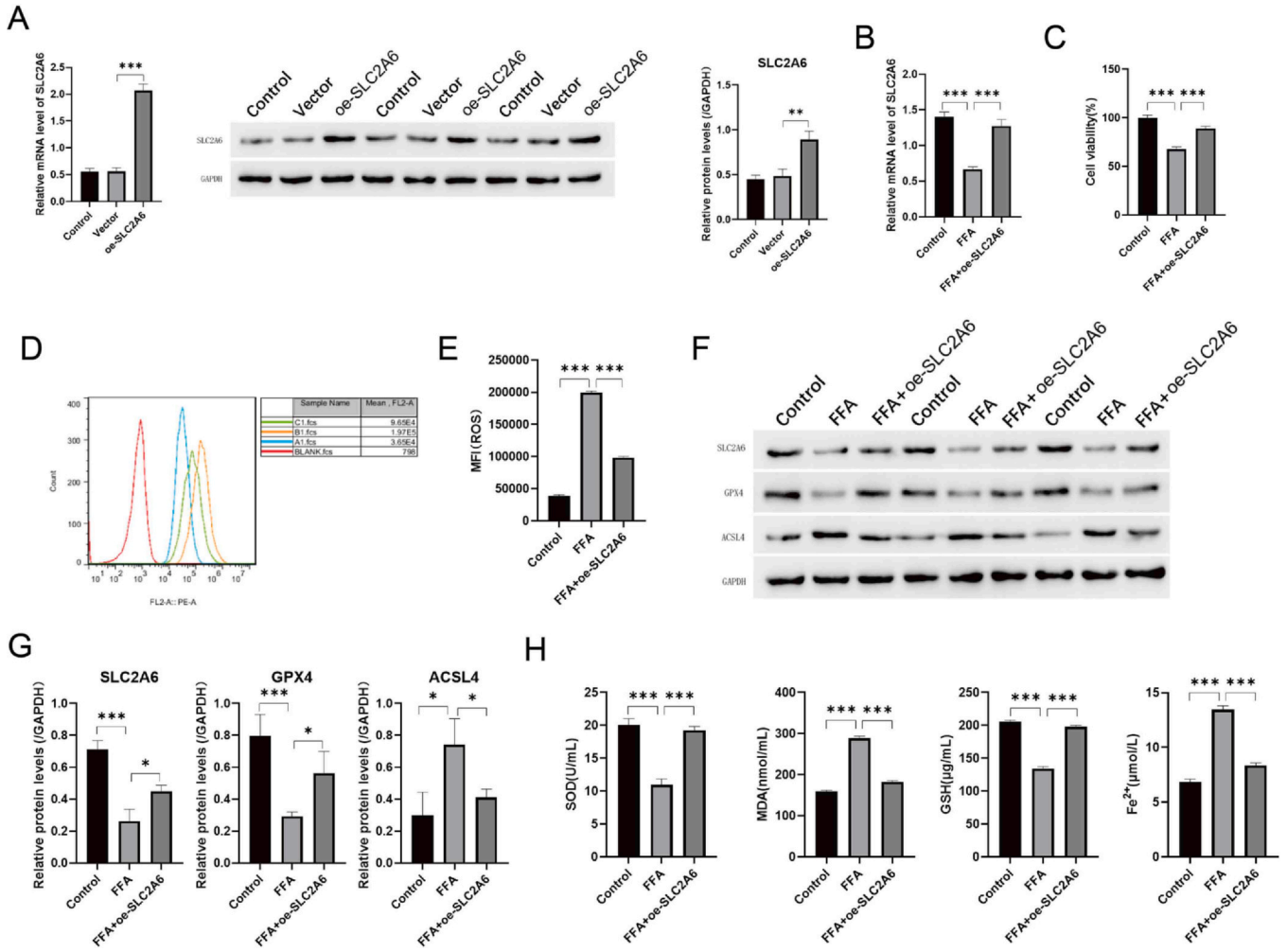

Fig. 4. Effects of *SLC2A6* overexpression on FFA-induced oxidative stress and ferroptosis in HepG2 cells. (A) qRT-PCR analysis of *SLC2A6* mRNA expression in control, FFA-treated, and FFA + *SLC2A6* overexpression (oe-SLC2A6) groups. (B) Western blot analysis of SLC2A6 protein levels, with GAPDH as a loading control. (C) CCK-8 assay for cell viability in control, FFA-treated, and FFA + oe-SLC2A6 groups. (D, E) Flow cytometry analysis of lipid ROS levels using mean fluorescence intensity (MFI) in different groups. (F) Western blot analysis of SLC2A6, GPX4, and ACSL4 protein expression in control, FFA, and FFA + oe-SLC2A6 groups, with GAPDH as a loading control. (G) Quantification of (F). (H) Quantification of SOD, MDA, GSH, and Fe^{2+} levels across different groups. Data are expressed as mean ± standard deviation. *p < 0.05, **p < 0.01, ***p < 0.001, n = 3.

cg02257517 increasing risk and *SLC2A6* expression showing a protective effect. Multi-omics analysis confirmed an inverse relationship between *SLC2A6* methylation and expression, suggesting hypermethylation suppresses *SLC2A6* expression, increasing NAFLD susceptibility. Critically, the downregulation of *SLC2A6* was further validated in an independent cohort of human liver biopsies (GSE126848), providing direct clinical evidence for its relevance in NAFLD pathophysiology. Functionally, in HepG2 cells, FFA treatment induced lipid accumulation, oxidative stress, and *SLC2A6* downregulation, while *SLC2A6* overexpression restored cell viability, reduced lipid ROS, and attenuated oxidative stress and ferroptosis, as evidenced by increased SOD, GSH, and GPX4 along with decreased MDA, ACSL4, and Fe^{2+} levels. These findings highlight *SLC2A6* as a potential therapeutic target for NAFLD progression to NASH and fibrosis.

In the integrative multi-omics analysis, ALOX12 exhibited significant associations with NAFLD risk, consistent with its established role in promoting ferroptosis through lipid peroxidation.[28,29] A more complex picture emerged for *MAPKAP1*. Our SMR analysis identified a protective causal link, suggesting that higher genetically-predicted *MAPKAP1* expression is associated with a lower risk of NAFLD. This finding is paradoxical, as it directly contradicts established literature where *MAPKAP1* is reported to have a pro-pathogenic role, for instance by promoting ferroptosis through *SLC7A11* inhibition [30] or by driving M2 macrophage polarization in the liver.[31] Further complicating this, our own validation analysis in the GSE126848 liver tissue cohort revealed that *MAPKAP1* mRNA levels are significantly upregulated in NAFLD patients compared to controls (Fig. S5). This direct tissue-level evidence aligns with the pro-pathogenic role described in the literature but is inconsistent with our SMR result. This discrepancy likely stems from the difference between systemic genetic effects captured by blood-based eQTLs and localized pathological changes within the liver. The protective signal from SMR may reflect a baseline systemic genetic tendency, whereas the upregulation in bulk liver tissue is likely driven by infiltrating immune cells, such as pro-fibrotic macrophages, where *MAPKAP1* may exert a dominant pro-pathogenic role.[32] This highlights a key limitation of using blood as a tissue proxy and suggests that the function of *MAPKAP1* is highly context-dependent.

Our results showed that hypermethylation at *SLC2A6* (cg02257517) was associated with decreased *SLC2A6* expression, contributing to increased NAFLD risk. Importantly, this finding was directly validated in the GSE126848 liver tissue cohort, where *SLC2A6* mRNA was significantly downregulated in NAFLD patients (Fig. S5), providing strong clinical support for our SMR-based discovery. This regulatory role mirrors findings in lung adenocarcinoma, in which *SLC2A6* hypermethylation suppresses its expression, promoting tumor progression,[33] highlighting its epigenetic significance in different diseases. *SLC2A6*, also named *GLUT6*, encodes a glucose transporter that regulates glucose transport in lysosomes,[34] impacting cellular energy balance, oxidative stress, and iron homeostasis,[35] which are critical factors in the ferroptotic process. Our cell experiments demonstrated that *SLC2A6* overexpression in HepG2 cells reversed FFA-induced oxidative stress and ferroptosis, improving cell viability, reducing lipid ROS, and restoring antioxidant, while decreasing MDA, ACSL4, and Fe^{2+} levels. Given that *SLC2A6* supports cell survival and glycolysis in cancer,[36] its role in NAFLD may involve glucose transport-driven lipogenesis, fructose uptake, and inflammatory pathways, exacerbating liver fat accumulation and disease progression.[37] These findings highlight *SLC2A6* as a potential epigenetic and metabolic regulator in NAFLD pathogenesis.

Although a direct link between *SLC2A6* and NAFLD in humans has not been established, other *SLC2A* family members, such as *SLC2A2 (GLUT2),*[38] *SLC2A5 (GLUT5),*[39] and *SLC2A8 (GLUT8),*[40] are known to contribute to NAFLD development by facilitating glucose and fructose uptake, leading to triglyceride accumulation, hepatic steatosis, and fibrosis through enhanced lipogenesis, oxidative stress, and inflammation. Additionally, *SLC2A1 (GLUT1)* serves as a biomarker for disease progression.[41] Interestingly, while these transporters are typically associated with promoting NAFLD, our findings suggest that *SLC2A6* may have a protective effect, indicating a potential divergence in the roles of *SLC2A* family members in NAFLD. Given that SLC2A6 is primarily localized on lysosomal membranes and does not directly mediate glucose uptake,[42] its reduced expression may impair lysosomal function, which, in turn, could disrupt cellular energy balance. This disruption could enhance susceptibility to NAFLD, as lysosomal dysfunction is known to impair lipid and cholesterol metabolism, leading to cholesterol accumulation, defective lipid degradation, and ultimately contributing to hepatic steatosis and NAFLD development.[43]

In this study, *PRKCA* (Protein Kinase C Alpha, *PKCα*) was also identified as a potential risk factor for NAFLD, with our SMR analysis showing that its increased expression was positively correlated with disease risk. This finding is biologically plausible, as *PRKCA* is known to regulate ferroptosis by activating the *MEK* pathway and influencing the stability of the *xCT* antiporter.[44,45] Although not directly implicated in NAFLD, its family members (*PKCβ* and *PKCδ*) are involved in hepatic lipid metabolism and insulin signaling.[46,47] Furthermore, *PRKCA* itself has been shown to promote inflammation and induce insulin resistance,[48–50] both of which are core mechanisms in NAFLD pathogenesis. Thus, our findings provide genetic evidence suggesting a causal role for *PRKCA* in NAFLD, likely by modulating pathways related to ferroptosis, inflammation, and metabolic dysregulation.

In conclusion, this study successfully identified *SLC2A6* as a critical, protective gene in NAFLD through a multi-omics SMR approach, with its downregulation confirmed in clinical liver samples and its protective function validated in cellular models. Nevertheless, several limitations should be acknowledged. First, our primary SMR analysis relied on blood-based eQTL data. The case of *MAPKAP1*, where the SMR signal contradicted direct tissue expression, highlights the inherent risk of using blood as a proxy for liver pathophysiology and underscores that some of our other findings require further liver-specific validation. Second, while our results support a protective role for *SLC2A6* against ferroptosis, the precise underlying molecular mechanism, such as the proposed SLC2A6-PPP-GPX4 axis, remains to be experimentally validated. Third, the inability to replicate some associations in external cohorts suggests that further validation in larger and more diverse populations is necessary.

Future research should therefore focus on (1) dissecting the cell-type-specific roles of our candidate genes within the liver microenvironment, (2) performing in-depth mechanistic studies to validate the proposed protective pathways, and (3) expanding genetic validation using liver-specific omics data from diverse populations. Addressing these questions will be crucial for translating our findings into a deeper biological understanding and potential therapeutic strategies for NAFLD.

Conclusion

This study identified *SLC2A6* as a critical gene involved in NAFLD risk. Cell experiments showed that *SLC2A6* overexpression mitigated FFA-induced oxidative stress and ferroptosis, suggesting its protective role in NAFLD. The findings highlight the importance of ferroptosis in NAFLD. Further research, including validation in diverse populations and the use of liver-specific omics data, is essential to confirm these associations and assess their clinical applicability.

List of abbreviations

NAFLD, non-alcoholic fatty liver disease
SMR, summary data-based Mendelian Randomization
NASH, non-alcoholic steatohepatitis
ROS, reactive oxygen species
GPX4, glutathione peroxidase 4
GWAS, genome-wide association studies
QTL, quantitative trait loci

mQTLs, methylation QTLs
eQTLs, expression QTLs
GTEx, Genotype-Tissue Expression
HEIDI, heterogeneity in dependent instruments

Declarations

Not applicable.

Authors' contributions

Weifeng Wu: Investigation, Formal analysis. **Yizhong Bao:** Conceptualization. **Ying Yuan:** Data curation. **Jianjun Zhang:** Writing – review & editing. **Yue Zhang:** Conceptualization. **Xiaohu Yang:** Writing – review & editing, Validation, Formal analysis. **Zhen Wang:** Writing – review & editing, Writing – original draft, Conceptualization. **Xiao Liu:** Writing – review & editing, Writing – original draft, Investigation, Formal analysis, Data curation, Conceptualization. **Huadi Zhou:** Methodology. **Chenhan Shou:** Investigation.

Ethics approval and consent to participate

As the study utilized publicly accessible databases, there was no requirement for ethics committee approval or informed consent from participants. All methods were performed in accordance with the relevant guidelines and regulations.

Consent for publication

Not applicable.

Availability of data and materials

All data generated or analyzed during this study are included in this published article.

Funding

Not applicable.

Declarations of Competing Interests

The authors declare no competing interests.

Acknowledgements

Not applicable.

Authors' other information

Not applicable.

Appendix A. Supporting information

Supplementary data associated with this article can be found in the online version at doi:10.1016/j.prmedi.2025.100063.

References

1. Mitra S, De A, Chowdhury A. Epidemiology of non-alcoholic and alcoholic fatty liver diseases. *Transl Gastroenterol Hepatol.* 2020;5:16.
2. Tacke F, Weiskirchen R. Non-alcoholic fatty liver disease (NAFLD)/non-alcoholic steatohepatitis (NASH)-related liver fibrosis: mechanisms, treatment and prevention. *Ann Transl Med.* 2021;9:729.
3. Geh D, Anstee QM, Reeves HL. NAFLD-associated HCC: progress and opportunities. *J Hepatocell Carcinoma.* 2021;8:223–239.
4. Mehta KJ, Farnaud SJ, Sharp PA. Iron and liver fibrosis: mechanistic and clinical aspects. *World J Gastroenterol.* 2019;25:521.
5. Henry L, Paik J, Younossi Z. M. the epidemiologic burden of non-alcoholic fatty liver disease across the world. *Aliment Pharmacol Ther.* 2022;56:942–956.
6. Huang DQ, El-Serag HB, Loomba R. Global epidemiology of NAFLD-related HCC: trends, predictions, risk factors and prevention. *Nat Rev Gastroenterol Hepatol.* 2021;18:223–238.
7. Muthiah MD, Cheng Han N, Sanyal AJ. A clinical overview of non-alcoholic fatty liver disease: a guide to diagnosis, the clinical features, and complications—what the non-specialist needs to know. *Diabetes Obes Metab.* 2022;24:3–14.
8. Raza S, Rajak S, Upadhyay A, Tewari A, Sinha RA. Current treatment paradigms and emerging therapies for NAFLD/NASH. *Front Biosci.* 2021;26:206.
9. Jonas W, Schürmann A. Genetic and epigenetic factors determining NAFLD risk. *Mol Metab.* 2021;50:101111.
10. Gensluckner S, Wernly B, Datz C, Aigner E. Iron, oxidative stress, and metabolic dysfunction—associated steatotic liver disease. *Antioxidants.* 2024;13:208.
11. González-Domínguez Á, et al. Iron metabolism in obesity and metabolic syndrome. *Int J Mol Sci.* 2020;21:5529.
12. Wu J, et al. Ferroptosis in liver disease: new insights into disease mechanisms. *Cell Death Discov.* 2021;7:276. https://doi.org/10.1038/s41420-021-00660-4
13. YH L. *Study on the mechanism of apoptosis induced by environmental endocrine disruptor nickel sulfate in thyroid and pancreatic tissues and cells in rats.* Lanzhou University; 2020.
14. Porcu E, et al. Mendelian randomization integrating GWAS and eQTL data reveals genetic determinants of complex and clinical traits. *Nat Commun.* 2019;10:3300.
15. Zhou N, et al. FerrDb V2: update of the manually curated database of ferroptosis regulators and ferroptosis-disease associations. *Nucleic Acids Res.* 2023;51:D571–D582.
16. Wu Y, et al. Integrative analysis of omics summary data reveals putative mechanisms underlying complex traits. *Nat Commun.* 2018;9:918.
17. Võsa U, et al. Large-scale cis-and trans-eQTL analyses identify thousands of genetic loci and polygenic scores that regulate blood gene expression. *Nat Genet.* 2021;53:1300–1310.
18. Pietzner M, et al. Mapping the proteo-genomic convergence of human diseases. *Science.* 2021;374:eabj1541.
19. Consortium G. The GTEx Consortium atlas of genetic regulatory effects across human tissues. *Science.* 2020;369:1318–1330.
20. Sun Z, et al. Genetic variants in HFE are associated with non-alcoholic fatty liver disease in lean individuals. *JHEP Rep.* 2023;5:100744.
21. Namjou B, et al. GWAS and enrichment analyses of non-alcoholic fatty liver disease identify new trait-associated genes and pathways across eMERGE Network. *BMC Med.* 2019;17:1–19.
22. Zhu Z, et al. Integration of summary data from GWAS and eQTL studies predicts complex trait gene targets. *Nat Genet.* 2016;48:481–487. https://doi.org/10.1038/ng.3538
23. Wu Y, et al. Integrative analysis of omics summary data reveals putative mechanisms underlying complex traits. *Nat Commun.* 2018;9:918. https://doi.org/10.1038/s41467-018-03371-0
24. Giambartolomei C, et al. Bayesian test for colocalisation between pairs of genetic association studies using summary statistics. *PLoS Genet.* 2014;10:e1004383. https://doi.org/10.1371/journal.pgen.1004383
25. Rasooly D, Peloso GM, Giambartolomei C. Bayesian genetic colocalization test of two traits using coloc. *Curr Protoc.* 2022;2:e627.
26. Zuber V, et al. Combining evidence from Mendelian randomization and colocalization: review and comparison of approaches. *Am J Hum Genet.* 2022;109:767–782.
27. Zhu Z, et al. Integration of summary data from GWAS and eQTL studies predicts complex trait gene targets. *Nat Genet.* 2016;48:481–487.
28. Chu B, et al. ALOX12 is required for p53-mediated tumour suppression through a distinct ferroptosis pathway. *Nat Cell Biol.* 2019;21:579–591.
29. Shi J-F, et al. Targeting ferroptosis, a novel programmed cell death, for the potential of alcohol-related liver disease therapy. *Front Pharmacol.* 2023;14:1194343.
30. Zheng Y-D, Zhang Y, Ma J-Y, Sang C-Y, Yang J-L. A Carabrane-type sesquiterpenolide carabrone from carpesium cernuum inhibits SW1990 pancreatic cancer cells by inducing ferroptosis. *Molecules.* 2022;27:5841.
31. Huang B, Yu Z, Cui D, Du F. MAPKAP1 orchestrates macrophage polarization and lipid metabolism in fatty liver-enhanced colorectal cancer. *Transl Oncol.* 2024;45:101941.
32. Huby T, Gautier EL. Immune cell-mediated features of non-alcoholic steatohepatitis. *Nat Rev Immunol.* 2022;22:429–443. https://doi.org/10.1038/s41577-021-00639-3
33. Zhang Y, Qin H, Bian J, Ma Z, Yi H. SLC2As as diagnostic markers and therapeutic targets in LUAD patients through bioinformatic analysis. *Front Pharmacol.* 2022;13:1045179.
34. Chen S-Y, et al. Investigating the expression and function of the glucose transporter GLUT6 in obesity. *Int J Mol Sci.* 2022;23:9798.
35. Song W, Li D, Tao L, Luo Q, Chen L. Solute carrier transporters: the metabolic gatekeepers of immune cells. *Acta Pharm Sin B.* 2020;10:61–78.
36. Byrne FL, et al. Metabolic vulnerabilities in endometrial cancer. *Cancer Res.* 2014;74:5832–5845.
37. Basaranoglu M, Basaranoglu G, Bugianesi E. Carbohydrate intake and nonalcoholic fatty liver disease: fructose as a weapon of mass destruction. *Hepatobiliary Surg Nutr.* 2015;4:109.
38. Mueckler M, Thorens B. The SLC2 (GLUT) family of membrane transporters. *Mol Asp Med.* 2013;34:121–138.
39. De Vito F, et al. Association between higher duodenal levels of the fructose carrier glucose transporter-5 and nonalcoholic fatty liver disease and liver fibrosis. *J Intern Med.* 2024;295:171–180.
40. DeBosch BJ, Chen Z, Saben JL, Finck BN, Moley KH. Glucose transporter 8 (GLUT8) mediates fructose-induced de novo lipogenesis and macrosteatosis. *J Biol Chem.* 2014;289:10989–10998.

41. Zhang W, et al. Exosome GLUT1 derived from hepatocyte identifies the risk of non-alcoholic steatohepatitis and fibrosis. *Hepatol Int.* 2023;17:1170–1181. https://doi.org/10.1007/s12072-023-10520-1
42. Maedera S, et al. GLUT6 is a lysosomal transporter that is regulated by inflammatory stimuli and modulates glycolysis in macrophages. *FEBS Lett.* 2019;593:195–208.
43. Du J, Ji Y, Qiao L, Liu Y, Lin J. Cellular endo-lysosomal dysfunction in the pathogenesis of non-alcoholic fatty liver disease. *Liver Int.* 2020;40:271–280.
44. Do Van B, et al. Ferroptosis, a newly characterized form of cell death in Parkinson's disease that is regulated by PKC. *Neurobiol Dis.* 2016;94:169–178.
45. Monteleone L, et al. PKCα inhibition as a strategy to sensitize neuroblastoma stem cells to etoposide by stimulating ferroptosis. *Antioxidants.* 2021;10:691.
46. Shu Y, et al. Hepatocyte-specific PKCβ deficiency protects against high-fat diet-induced nonalcoholic hepatic steatosis. *Mol Metab.* 2021;44:101133.
47. Zhang J, et al. PKCδ regulates hepatic triglyceride accumulation and insulin signaling in Leprdb/db mice. *Biochem Biophys Res Commun.* 2014;450:1619–1625.
48. Yang J, et al. Adipose transplantation improves olfactory function and neurogenesis via PKCα-involved lipid metabolism in Seipin Knockout mice. *Stem Cell Res Ther.* 2023;14:239.
49. Leppänen T, Tuominen RK, Moilanen E. Protein kinase C and its inhibitors in the regulation of inflammation: inducible nitric oxide synthase as an example. *Basic Clin Pharmacol Toxicol.* 2014;114:37–43.
50. Mishra D, Reddy I, Dey CS. PKCα Isoform inhibits insulin signaling and aggravates neuronal insulin resistance. *Mol Neurobiol.* 2023;60:6642–6659.